Quart. J. R. Met. Soc. (1975), **101**, pp. 313–324

551.515.31

A numerical study of boundary effects on concentrated vortices with application to tornadoes and waterspouts

By L. BODE* and L. M. LESLIE and R. K. SMITH

Department of Applied Mathematics, University of Edinburgh, Edinburgh

Commonwealth Meteorology Research Centre, P.O. Box 5089, Melbourne, Australia, 3001

Department of Mathematics, Monash University, Clayton, Australia, 3168

(Received 13 September 1974)

SUMMARY

This paper extends the numerical study of the structure and development of a concentrated vortex by Leslie (1971), in which a vortex is simulated by suddenly imposing an upwards body force along a section of the vertical axis of a contained rotating fluid, initially in a state of uniform rotation. Whereas the former paper was concerned primarily with demonstrating the prediction of Morton (1969) that a concentrated vortex may be generated only for a restricted range of the flow parameters, the present paper investigates the important role of boundaries on vortex behaviour.

Particular interest is focused on the boundary which is normal to the vortex core and 'behind' the body force. On this boundary the surface stress is related to the surface velocity by a drag coefficient C_D and experiments are performed in which C_D is infinite, unity and zero corresponding with a no-slip, a partially yielding and a free-slip boundary respectively. These calculations are motivated by the desire to assess what differences, if any, between tornadoes (which develop over land) and waterspouts (which develop over the sea) can be attributed to the different surface constraint. We also study the effect on a vortex due to an abrupt change in surface condition as this is relevant to the behaviour of a tornado which happens to cross a water surface, or even one which traverses ground with varying roughness characteristics, and conversely to the behaviour of a waterspout which moves over land.

It is shown that the strength of the meridional circulation associated with the vortex, and hence the strength of the upflow in the vortex itself, are increasing functions of the surface stress. On the other hand, the azimuthal kinetic energy, and in particular the strength of the vortex as measured by the maximum swirling velocity attained, decreases as the surface stress increases. Moreover, if the drag coefficient is suddenly increased, the meridional circulation increases, the azimuthal kinetic energy decreases and the vortex width (as measured by the radius of the maximum swirling velocity at a given height) increases. These effects are reversed if the drag coefficient is decreased and do not depend on the frictional effect of the container side wall. The role of the side wall itself is briefly explored.

The results accord with the behaviour of laboratory vortices formed in air over surfaces of different roughness as studied by Dessens (1972). They also appear consistent with the observation reported by Golden (1971, p. 146) concerning the behaviour of a waterspout whose circulation decreased rapidly and visible funnel expanded during a traverse of about a kilometre over land and which subsequently reformed on moving back over water.

1. INTRODUCTION

In the last few years there has been a proliferation of attempts at modelling concentrated vortex flows in the hope that such studies will provide insight into the mechanics of tornadoes, the most locally destructive of all atmospheric phenomena, and waterspouts, their less violent maritime counterparts. Since very little is known about the detailed structure of these atmospheric vortices, or the processes responsible for their formation, and because of the enormous difficulties and hazards of acquiring field data, especially on tornadoes, the model studies have a particularly important role to play in aiding understanding.

Two principal flow features that appear necessary for vortex formation are a region of fluid rich in ambient rotation, and hence vorticity, and an independently driven motion which produces convective acceleration along vortex lines, and therefore amplification of

* Present address: Department of Mathematics, University of Papua and New Guinea, P.O. Box 4820, University, Papua, New Guinea.

vorticity, in a subregion of the fluid. In most simulation experiments (including both laboratory and numerical studies) fluid is contained in a cylindrical region and ambient rotation is maintained by the rotation of some or all of the container boundaries about the axis of symmetry. An alternative but largely equivalent means of providing an angular momentum source is used by Fitzgarrald (1973) in which swirl is imparted to converging fluid at low levels by a series of vanes inclined to the radial direction, whereas Davies-Jones and Vickers (1971) study transient vortices generated in an unmaintained field of rotating fluid. In some experiments the container sidewall is rigid and in others the rotating portion of the sidewall is porous and air acquires angular momentum as it enters through this boundary. A variety of driving mechanisms have been used, including axial suction (Long 1958; Ying and Chang 1970; Wan and Chang 1972; Ward 1972; Dessens 1972), buoyant convection (Emmons and Ying 1967; Davies-Jones and Vickers 1971; Fitzgarrald 1973) and an axial body force (Turner and Lilly 1963; Turner 1966; Leslie 1971; Bode 1973).

Although ambient rotation, together with some type of forcing as described above, appear prerequisites for concentrated vortex formation, they are by no means sufficient. Thus, according to the theoretical analysis of Morton (1969), for a given level of ambient rotation, characterized by some measure of the gross circulation, a concentrated vortex may be sustained only if the axial flow force lies within certain limits. If the forcing is too large, rotation plays only a minor role in the flow behaviour and if it is too low, the motion is strongly inhibited by rotation except in the locality of the forcing region. These predictions are confirmed by the numerical experiments of Leslie (1971) and by laboratory studies (see in particular Long 1958; Fitzgarrald 1973).

Another feature known to be of major importance in vortex dynamics is the constraint on the flow due to a boundary normal to the vortex core. In the case of a tornado, this boundary is the ground and for a waterspout it is the sea surface. Not only does this boundary support the low pressure associated with the vortex centre, its frictional influence serves to disrupt the approximate balance between centrifugal forces and the radial pressure gradient which exists in the vortex core at larger heights. Since vertical accelerations are small close above the boundary, the radial pressure field of the vortex is not significantly affected whereas centrifugal forces are reduced by friction in a shallow boundary layer. The resulting imbalanced pressure field drives a strong inflow in this layer and because of symmetry, this is diverted to produce upflow in at least the lower part of the core. The strength of upflow depends on the strength of inflow which in turn depends on the net radial pressure gradient at lower levels and hence on the strength of the swirling velocity field just above the boundary layer. Consequently the axial flow is intimately coupled with the azimuthal motion in the core in the neighbourhood of the boundary; moreover the effect of this boundary induced constraint is felt for a considerable distance along the core (Morton 1966).

In this paper we describe a series of numerical experiments based on the model of Leslie (1971) which are used to explore the effect of boundaries on vortex evolution and strength. For reasons described above, interest is focussed largely on the lower boundary on which the vortex terminates and a primary aim is to assess to what extent, if at all, the different nature of the surface in the case of tornadoes and waterspouts, can account for the observed difference in strength between these vortices. We also seek to explore the possible changes which occur as a tornado crosses to a water surface, or one with markedly different roughness characteristics and conversely, when a waterspout moves over land.

2. Equations of motion

The essential features of the model are shown in Fig. 1. Homogeneous, viscous fluid of

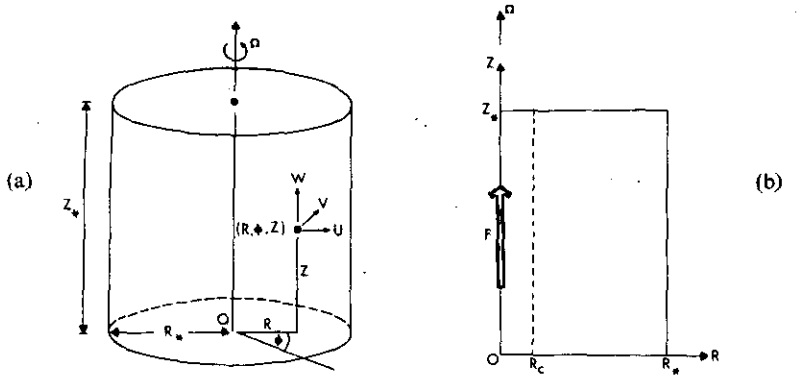

Figure 1. (a) Sketch of the flow configuration and of the co-ordinate system used. (b) Corresponding cross-section in the R,Z plane showing the vertical location (arrow) and radial extent ($R < R_c$) of the imposed body force.

density ρ and kinematic viscosity ν is contained in a circular cylinder of radius R_* and height Z_* which rotates about its vertical axis with angular velocity Ω. The flow is driven by an applied upward body force of magnitude $F(R)$, centred on the middle third of the axis and distributed over a radius R_c (Fig. 1(b)) and the motion is described in terms of velocity components (U, V, W) referred to a cylindrical co-ordinate system (R, ϕ, Z) which rotates with the cylinder.

The dynamic pressure P is related to the total pressure P_* by the formula $P = P_* + \rho g Z - \frac{1}{2}\rho R^2\Omega^2$; and since F is taken to be independent of azimuth angle, axi-symmetric flow is presumed to occur.

If representative length and velocity scales, R_c and $W_* = (F(0)R_c)^{\frac{1}{2}}$, are chosen for the vortex motion, appropriate scales for time T and dynamic pressure are R_c/W_* and ρW_*^2 and the model is characterized by four dimensionless parameters: a Rossby number, $Ro = W_*/2\Omega R_c$; a Reynolds number, $Re = W_* R_c/\nu$ and the pair of aspect ratios R_c/R_*, Z_*/R_*.

With lower-case letters denoting dimensionless variables with respect to the scales defined above, the Navier-Stokes equation and equation of continuity appropriate to the flow described take the form

$$\frac{\partial u}{\partial t} + u\frac{\partial u}{\partial r} + w\frac{\partial u}{\partial z} - \left(\frac{1}{Ro} + \frac{v}{r}\right)v = -\frac{\partial p}{\partial r} + \frac{1}{Re}\left[\frac{\partial^2 u}{\partial z^2} + \frac{\partial}{\partial r}\left(\frac{1}{r}\frac{\partial}{\partial r}(ru)\right)\right], \quad (1)$$

$$\frac{\partial v}{\partial t} + u\frac{\partial v}{\partial r} + w\frac{\partial v}{\partial z} + \left(\frac{1}{Ro} + \frac{v}{r}\right)u = \frac{1}{Re}\left[\frac{\partial^2 v}{\partial z^2} + \frac{\partial}{\partial r}\left(\frac{1}{r}\frac{\partial}{\partial r}(rv)\right)\right], \quad (2)$$

$$\frac{\partial w}{\partial t} + u\frac{\partial w}{\partial r} + w\frac{\partial w}{\partial z} = f - \frac{\partial p}{\partial z} + \frac{1}{Re}\left[\frac{\partial^2 w}{\partial z^2} + \frac{1}{r}\frac{\partial}{\partial r}\left(r\frac{\partial w}{\partial r}\right)\right], \quad (3)$$

$$\frac{\partial}{\partial r}(ru) + \frac{\partial}{\partial z}(rw) = 0, \quad (4)$$

where $f(r) = F(R_c r)/F(0)$. In non-dimensional units, the tank dimensions are $r_* = R_*/R_c$ and $z^* = Z^*/R_c$ respectively.

Eqs. (1) to (4) can be simplified by introducing a streamfunction ψ, so that $u = -r^{-1}\partial\psi/\partial z$ and $w = r^{-1}\partial\psi/\partial r$, and the zonal vorticity component defined by $\zeta = \partial u/\partial z - \partial w/\partial r$. In terms of ψ, ζ and v, the set of equations to be solved reduces to

$$\frac{\partial \zeta}{\partial t} + \mathrm{J}\left(\frac{\zeta}{r}\right) = -\frac{\partial f}{\partial r} + \left(\frac{1}{Ro} + \frac{2v}{r}\right)\frac{\partial v}{\partial z} + \frac{1}{Re}\left\{\frac{\partial^2 \zeta}{\partial z^2} + \frac{\partial}{\partial r}\left[\frac{1}{r}\frac{\partial}{\partial r}(r\zeta)\right]\right\}, \quad (5)$$

$$\frac{\partial v}{\partial t} + \frac{1}{r}\mathrm{J}(v) = \left(\frac{1}{Ro} + \frac{v}{r}\right)\frac{1}{r}\frac{\partial \psi}{\partial z} + \frac{1}{Re}\left\{\frac{\partial^2 v}{\partial z^2} + \frac{\partial}{\partial r}\left[\frac{1}{r}\frac{\partial}{\partial r}(rv)\right]\right\}, \quad (6)$$

and

$$\zeta = -\frac{\partial}{\partial r}\left(\frac{1}{r}\frac{\partial \psi}{\partial r}\right) - \frac{1}{r}\frac{\partial^2 \psi}{\partial z^2}, \quad (7)$$

where

$$\mathrm{J}(\theta) \equiv \frac{\partial \psi}{\partial r}\frac{\partial \theta}{\partial z} - \frac{\partial \psi}{\partial z}\frac{\partial \theta}{\partial r}.$$

3. Boundary conditions

The conditions imposed at the boundaries of the computational domain are:

(i) $r = 0$: symmetry at the axis of rotation implies that $\zeta = v = \psi = 0$.

(ii) $z = 0$: three different boundary conditions are examined corresponding with no-slip (case A); a yielding surface with finite but non zero stress (case B); and a stress-free (free-slip) surface (case C). In all cases the bottom boundary is assumed to be flat. These boundary conditions can be grouped by the general formula

$$\frac{\partial \mathbf{u}_0}{\partial z} = Re\, C_D\, |\mathbf{u}_0|\, \mathbf{u}_0, \quad (8)$$

where $\mathbf{u}_0 = (u_0, v_0, 0)$ denotes the velocity vector at $z = 0$ and C_D is a drag coefficient which is arbitrarily large in case A, finite in case B and zero in case C. In terms of ζ, v and ψ, the condition at $z = 0$ becomes

case A: $\zeta = -\frac{1}{r}\frac{\partial^2 \psi}{\partial z^2}, \quad u = 0, \quad v = 0, \quad \psi = 0;$

case B: $\zeta = C_D\, |\mathbf{u}_0|\, u_0, \quad \frac{\partial v}{\partial z} = C_D\, |\mathbf{u}_0|\, v_0, \quad \psi = 0;$

case C: $\zeta = 0, \quad \frac{\partial v}{\partial z} = 0, \quad \psi = 0.$

(iii) $r = r_*$: at the side boundary, corresponding with the cylinder wall, either a no-slip (case α) or free-slip (case β) condition is taken, i.e.

case α: no-slip: $\zeta = \frac{1}{r}\frac{\partial^2 \psi}{\partial r^2}, \quad v = 0, \quad \psi = 0;$

case β: free-slip: $\zeta = 0, \quad \frac{\partial v}{\partial r} = 0, \quad \psi = 0.$

(iv) $z = z_*$: At the upper boundary a stress-free condition is taken, i.e. $\zeta = 0$, $\frac{\partial v}{\partial z} = 0$, $\psi = 0$.

4. Numerical method

The numerical method is essentially the same as that described by Leslie (1971) and

only a brief presentation is needed here. Eqs. (5) to (7) are replaced by the finite-difference analogues:

$$\delta_t \bar{\zeta}^t + J_A(\zeta/r) = -\delta_r \bar{f}^r + \frac{1}{Ro}\delta_z \bar{v}^z + \frac{1}{r}\delta_z(\overline{v^2}^z) + \frac{1}{Re}\left\{\delta_{zz}\zeta + \delta_r\left[\frac{1}{r}\delta_r(r\zeta)\right]\right\}, \quad (9)$$

$$\delta_t \bar{v}^t + \frac{1}{r} J_A(v) = \frac{1}{r}\delta_z \bar{\psi}^z\left(\frac{1}{Ro} + \frac{v}{r}\right) + \frac{1}{Re}\left\{\delta_{zz}v + \delta_r\left[\frac{1}{r}\delta_r(rv)\right]\right\}, \quad (10)$$

$$\zeta = -\delta_r\left(\frac{1}{r}\delta_r\psi\right) - \frac{1}{r}\delta_{zz}\psi, \quad (11)$$

where, in usual notation,

$$\bar{\theta}^x = \tfrac{1}{2}[\theta(x + \tfrac{1}{2}\Delta x) + \theta(x - \tfrac{1}{2}\Delta x)], \quad \theta_x = \frac{1}{\Delta x}[\theta(x + \tfrac{1}{2}\Delta x) - \theta(x - \tfrac{1}{2}\Delta x)].$$

The Jacobian operator $J_A(\theta)$ is the Arakawa conserving operator used by Williams (1967) in his numerical study of thermal convection in a rotating annulus. It is also noted that the diffusion terms of Eqs. (9) and (10) are evaluated at preceding time levels to prevent computational instability arising from these terms.

5. Selection of the flow parameters

In all the numerical experiments, the container dimensions are $R_* = 7{\cdot}5$cm and $Z_* = 30$ cm and the finite difference equations are solved over a mesh with 24 radial and 96 vertical grid spacings. The width of the forcing region is two grid spacings from the axis; i.e. $R_c = 0{\cdot}625$cm.

As noted in section 1, there is a restricted range of the governing parameters for which a concentrated vortex will form and some preliminary experimentation, guided by the analysis of Morton (1969), proved necessary to determine suitable parameters in this range. The values chosen are $F(0) = 1{\cdot}5\text{cm}^2\,\text{s}^{-1}$, $\Omega = 0{\cdot}1\text{s}^{-1}$ and $\nu = 1{\cdot}002 \times 10^{-2}\text{cm}^2\,\text{s}^{-1}$ (the kinematic viscosity of water at 20°C) and the corresponding approximate values of W_*, Ro and Re are $0{\cdot}97\text{cm}\,\text{s}^{-1}$, 15·5 and 60·5 respectively. These parameters lead to a vortex flow exhibiting large amplification (of up to two orders of magnitude) of the background rotation, measured by the maximum swirling velocity attained V_m, compared with the swirling velocity ΩR_m, due to solid body rotation with angular speed Ω, at the radius R_m at which this maximum occurs.

In contrast to the earlier model (Leslie 1971) the body force is situated along the middle third of the axis in order to minimize, as far as possible, the direct influence of forcing in the vicinity of the top boundary. The body force profile $f(r)$ is taken to decrease linearly from its maximum value on the axis to zero at $r = 1$ (i.e. $R = R_c$).

In all the calculations, a non-dimensional time step of 0·03 is found to be sufficient to ensure computational stability and in most experiments, a quasi-steady state is reached after about 5000 time steps.

6. The numerical experiments

The following discussion is based on the results of seven experiments in which different combinations of lower and sidewall boundary conditions are imposed. These experiments are summarized in Table 1.

(*a*) *Vortex evolution*

The evolution of vortex structure is exemplified in all cases by that of experiment Aα in which no-slip boundary conditions are imposed on both the lower and sidewall boundaries. Two stages in the flow development are illustrated in Figs. 2 and 3 which compare the streamline patterns and isotachs of the three velocity components after 1000 and 5000 time steps, representing conditions before the vortex interacts noticeably with the lower boundary and those in the quasi-steady, mature stage, respectively.

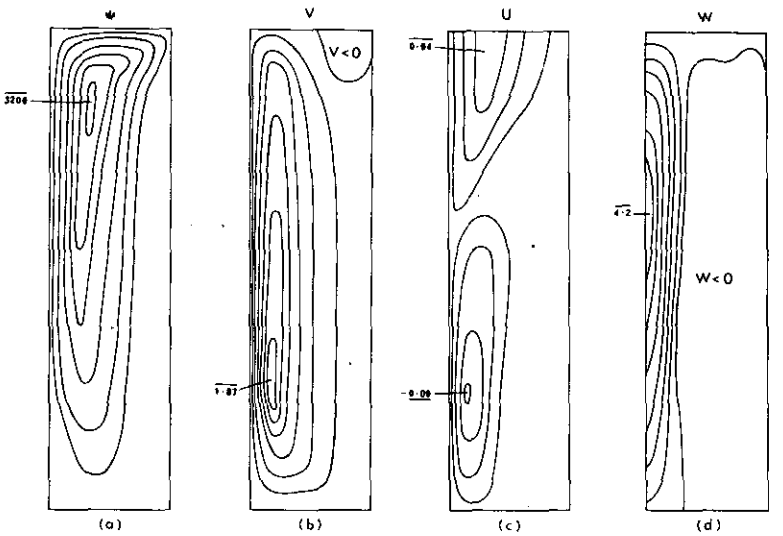

Figure 2. Vortex structure in expt. Aα (i.e. no-slip on the lower boundary and side wall) after 1000 time steps before the vortex interacts noticeably with the lower boundary. The streamlines are shown in (a) and isotachs of azimuthal, radial and vertical velocity components in (b), (c) and (d) respectively.

The process of evolution may be summarized briefly as follows. Immediately after the body force is applied, a local meridional circulation is induced and fluid is drawn radially inwards in the vicinity of the lower half of the forcing region. Since angular momentum is conserved, this fluid acquires cyclonic rotation relative to the tank leading to the formation of a local balance between centrifugal forces with the radial pressure gradient. (Note: the formation of this balance is assured by our choice of forcing strength in relation to background rotation rate as discussed in section 5; if the forcing is too small, the induced radial pressure gradient is insufficient to support the relatively strong centrifugal force field and if the forcing is too strong, centrifugal forces will be insufficient to balance the relatively strong radial pressure gradient and in either case, a concentrated vortex will not form.) This balance inhibits additional radial entrainment by the body force at that level and free or relatively free radial entrainment becomes possible only at successively smaller heights. Thus the vortex extends progressively downwards until it begins to interact with the lower boundary, leading to establishment of a well-defined inflow boundary layer.

The principal features of the mature circulation include a narrow vortex core of intense cyclonic rotation surrounding the axis, with upflow along its entire length and significant inflow confined to a shallow boundary layer adjacent to the lower boundary; a high level outflow region over much of which there is anticyclonic rotation (relative to the tank), due again to angular momentum conservation, and a broad region of downflow outside the vortex which completes the meridional circulation. In this experiment, the maximum amplification of the background rotation (as measured by $V_m/\Omega R_m$ – see section 5) is 72.

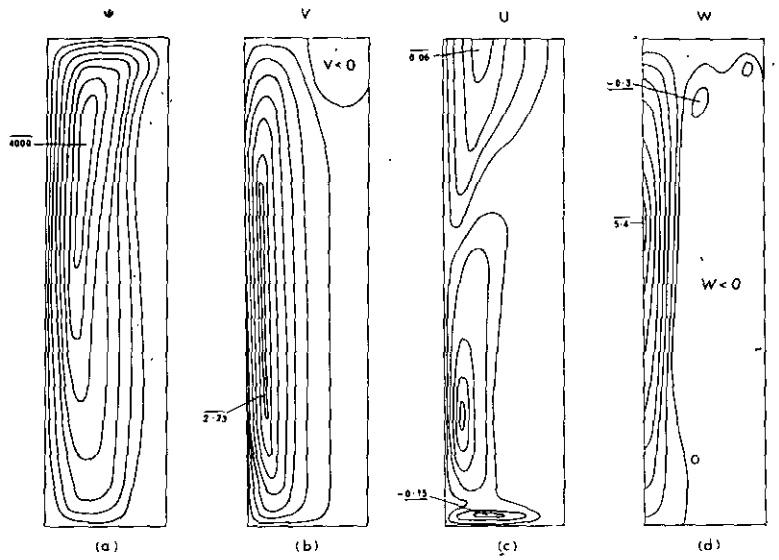

Figure 3. Vortex structure in expt. Aα after 5000 time steps when a quasi-steady state is attained. This should be compared with Fig. 2. The strong inflow boundary layer due to interaction of the core with the lower boundary is clearly pronounced in the radial isotach pattern (c).

It is pertinent to note that in all the experiments so far reported (both laboratory and numerical) in which a vortex is driven by a body force located along part of the axis of rotation, the vertical motion is directed upwards along the entire axis. However, in all these experiments, the lower boundary is relatively close to the forcing region and it is still uncertain whether or not it is possible to produce axial stagnation and a region of downflow along the axis, by increasing the vertical extent of the flow domain below the forcing region whilst keeping the depth and position of the forcing region fixed. This would presumably allow greater axial flow development with reduced axial constraint due to particular structure of forcing. The capacity of our present computing facilities have so far precluded us from investigating this point.

It is also evident that there are greater constraints on vortex development in axially forced vortices than in buoyancy driven vortices where there is maximum freedom for the vortex to select its own radial length scale and pattern of upflow (which may not be concentrated at the axis). Regions of axial downflow are therefore more likely to occur in buoyancy driven vortices and are observed in laboratory experiments (Fitzgarrald 1973).

These considerations are very important in any attempts to relate our numerical experiments to atmospheric vortices – see section 7.

(*b*) *Effect of the lower boundary*

The importance of the lower boundary on vortex dynamics is discussed in section 1. In our numerical experiments we investigate differences in the structure and intensity of the vortex according to the amount of drag exerted by this boundary. In doing this, all other parameters, in particular the strength of forcing and rotation rate of the container, are held fixed. Comparison is made between a lower boundary at which there is no-slip (expt. Aα), corresponding with an arbitrarily large value of C_D in Eq. (8), and boundaries which allow partial yielding ($C_D = 1$; expt. $B_1\alpha$) and free-slip ($C_D = 0$, expt. Cα). The principal differences in flow behaviour at the mature stage of development are indicated in Figs. 4, 5, 6 and in Table 2.

TABLE 1. DETAILS OF BOUNDARY CONDITIONS USED IN THE NUMERICAL EXPERIMENTS

Experiment name	Lower boundary condition	Side wall boundary condition	Upper boundary condition
$A\alpha$	No-slip	No-slip	Free slip
$B_1\alpha$	Slip ($C_D = 1{\cdot}0$)	No-slip	Free slip
$B_2\alpha$	Slip ($C_D = 0{\cdot}1$)	No-slip	Free slip
$C\alpha$	Free slip	No-slip	Free slip
$A\beta$	No-slip	Free slip	Free slip
$B_1\beta$	Slip ($C_D = 1{\cdot}0$)	Free slip	Free slip
$B_2\beta$	Slip ($C_D = 0{\cdot}1$)	Free slip	Free slip

TABLE 2. QUASI-STEADY-STATE KINETIC ENERGY PARTITION BETWEEN MERIDIONAL AND AZIMUTHAL CIRCULATIONS FOR THE NUMERICAL EXPERIMENTS OF TABLE 1

Experiment Name	Meridional kinetic energy/unit mass (cm^2s^{-2})	Azimuthal kinetic energy/unit mass (cm^2s^{-2})	Total kinetic energy/unit mass (cm^2s^{-2})
$A\alpha$	$1{\cdot}20 \times 10^3$	$1{\cdot}11 \times 10^3$	$2{\cdot}31 \times 10^3$
$B_1\alpha$	$0{\cdot}98 \times 10^3$	$1{\cdot}38 \times 10^3$	$2{\cdot}36 \times 10^3$
$B_2\alpha$	$0{\cdot}92 \times 10^3$	$1{\cdot}52 \times 10^3$	$2{\cdot}44 \times 10^3$
$C\alpha$	$0{\cdot}83 \times 10^3$	$1{\cdot}71 \times 10^3$	$2{\cdot}54 \times 10^3$
$A\beta$	$1{\cdot}32 \times 10^3$	$1{\cdot}42 \times 10^3$	$2{\cdot}74 \times 10^3$
$B_1\beta$	$1{\cdot}15 \times 10^3$	$1{\cdot}68 \times 10^3$	$2{\cdot}83 \times 10^3$
$B_2\beta$	$1{\cdot}11 \times 10^3$	$1{\cdot}77 \times 10^3$	$2{\cdot}88 \times 10^3$

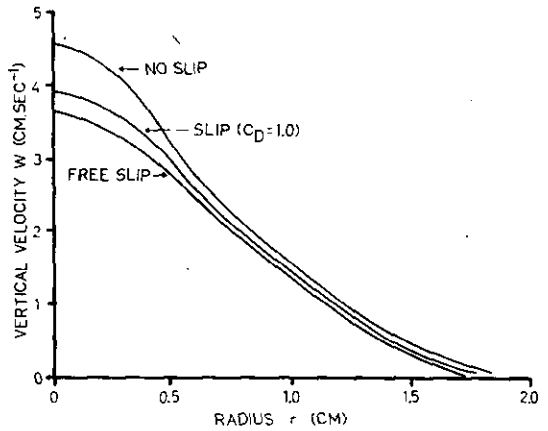

Figure 4. Radial profiles of vertical velocity at a height of 10cm in the tank in expts. $A\alpha$, $B_1\alpha$, $C\alpha$, in the quasi-steady state.

Figs. 4 and 5 show radial profiles of vertical and azimuthal velocity respectively at a height of 10cm above the lower boundary in the three experiments and Table 2 lists the total kinetic energy and its partition into azimuthal and meridional kinetic energy in all the experiments listed in Table 1, including the above three. Finally, Fig. 6 shows the streamline pattern and isotachs of the azimuthal, radial and vertical velocity components in expt. $C\alpha$ and the reader should compare these with the corresponding parts of Fig. 3.

On the basis of these figures and Table 2, the following deductions are possible. Smaller (larger) values of the surface drag (as measured by the value of C_D) are associated with smaller (larger) vertical velocities but with larger (smaller) azimuthal velocities and narrower

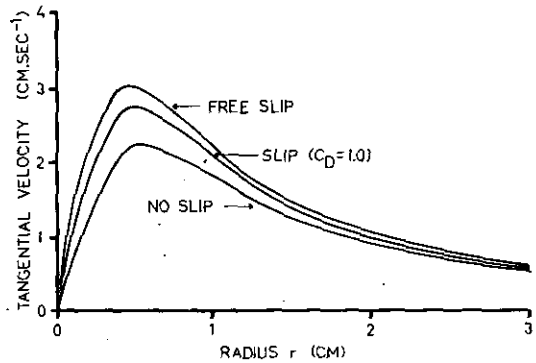

Figure 5. Radial profiles of tangential (azimuthal) velocity at a height of 10cm in the tank in expts. Aα $B_1\alpha$, Cα, in the quasi-steady state.

(broader) vortex cores (as measured by the radius of the maximum swirling velocity at a given height).

The first deduction seems consistent with the simple physical idea that for smaller surface drag, there is less frictional disruption of the cyclostrophic force balance of the vortex within the boundary layer and therefore less induced convergence within this layer, but it tacitly assumes that any concomitant change in the vortex structure to accommodate

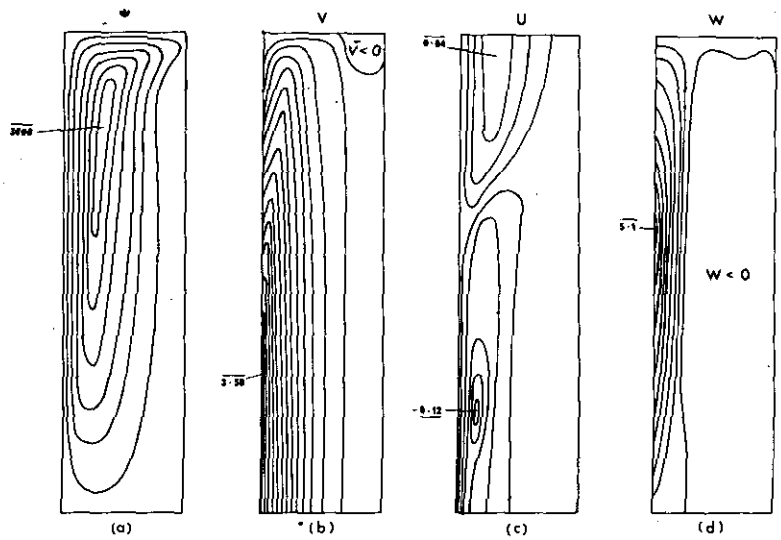

Figure 6. Vortex structure in expt. Cα (i.e. free-slip on the lower boundary and no-slip on the side wall) after 5000 time steps. Otherwise legend as in Fig. 2. This should be compared with Fig. 3. Note: with free-slip there is minimal interaction of the vortex core with the lower boundary and no inflow boundary layer exists.

the weaker inflow can be neglected. Such an assumption can be misleading and to be certain of the effect one must do the calculation. It turns out that this effect does occur as is dramatically illustrated by comparing the radial velocity isotachs in Figs. 3 and 6: in the former case, there is a well marked boundary layer of low level convergence, whereas in the latter, this feature is noticeably absent. For similar reasons, owing to the strong interdependence of the core flow with that in the boundary layer, it does not seem possible to make the second and third deductions on the basis of simple physical arguments, and

again it is necessary to perform the calculation. It is certainly true, as may be seen in Table 2, that a larger surface drag corresponds with a larger frictional torque and therefore with a smaller level of azimuthal kinetic energy, as expected. But we have seen that it also corresponds with an enhanced meridional circulation due to boundary layer convergence. This, in turn, is associated with larger convective accelerations which *may* lead to increased local generation of vorticity, and therefore higher swirling velocities in the core. In these experiments, it happens that the frictional effect is more important and although this may be true in all vortex flows (it appears also to be the case in the laboratory vortices studied by Dessens (1972) and in the calculations of Rosenthal (1971) concerning the constraint of surface drag in tropical cyclones) the evidence available so far may not be regarded as conclusive. Indeed, we are unable to subscribe to the bold assertions of Brooks (1951), who seems to regard these effects as self-evident.

The results described above can also be used to predict the change in vortex behaviour due to a sudden change in surface drag (we have in fact performed calculations in which the drag was suddenly increased or decreased but these calculations, apart from giving an indication of the spin-up/spin-down time to a new steady state (about 1000 time steps in each case) do not provide significant new information) and although we are cautious in suggesting that our vortices relate *directly* to tornadoes or waterspouts as far as their surface termination is concerned, it is this potential application which has motivated us. Moreover, it is interesting that the behaviour on drag as described above appears to corroborate an observation by Golden (1968, 1971) of a waterspout that made landfall and '. . . soon afterward resembled a large dust devil. The circulation at low levels decreased rapidly after moving over land, and the visible funnel expanded, became very hollow and translucent, and gradually retracted into the parent cloud. However, this average-sized waterspout maintained its vortical identity while crossing some 1100yd of flat land and reformed after moving off the north shore of the Key.' Of course, on moving over land, flow visualization changes from water droplets to particles of dust, especially at low levels, and this gives rise to some uncertainty in the observation. Nevertheless, it is not unreasonable to suppose that the radius of the visible spray vortex and that of the dust column are broadly characteristic of the radii of strongest swirling velocity close above the sea surface or ground, respectively.

(c) *Effect of the side wall*

The nature of the side wall boundary condition has implications regarding the angular momentum budget of the system. In the case of a no-slip condition on this boundary, the side wall can act as a source and/or sink of angular momentum whereas with a free-slip condition, angular momentum cannot be exchanged with the side wall and can only enter or leave the system through the lower boundary. (Note: if a free-slip lower boundary condition is used in conjunction with a similar condition on the side wall, there is insufficient internal dissipation to produce a steady state in the system in an acceptable computational time. However, this problem is not particularly relevant from a physical viewpoint: in the absence of boundary dissipation, a high level of meridional kinetic energy can be attained whereas the azimuthal kinetic energy can only decrease as there is no net torque on the system.) Some effects of relaxing the side wall boundary condition are indicated in Table 2. Briefly, with free-slip instead of no-slip on the side wall, there is less dissipation of meridional and azimuthal kinetic energy but the systematic effect of decreasing surface roughness is the same as described in section 6(*b*). There is also a larger region of anticyclonic circulation associated with the upper level outflow (diagram not shown) and this is consistent with the absence of torque at this boundary.

7. Conclusion

This paper explores the effect of the lower boundary on the dynamics of a particular type of concentrated vortex with a particular geometry and shows that a decrease in drag at this boundary causes the vortex to tighten and spin faster but reduces the strengths of the frictionally induced inflow and hence the vertical flow in the core. These effects are reversed if the surface drag is increased. Although many workers regard these effects as self-evident (see e.g. Brooks 1951), we believe that they cannot be simply inferred on the basis of physical arguments in view of the intimate coupling between the vortex core and its terminating lower boundary layer. Thus, calculations of this kind, supported by laboratory experimentation and careful field observation, are essential to a furtherance of our understanding of atmospheric vortices such as tornadoes and waterspouts.

The results of our study corroborate the behaviour of the laboratory vortices reported by Dessens (1972) and if certain assumptions are made regarding the change in flow visualization (see section 6(*b*)) they appear consistent with the observation reported by Golden (1971) concerning the modification of a waterspout which made landfall.

There are, of course, major differences between these vortices and those of our model; in particular, the former exist in the turbulent regime and although Dessens observes upflow in the core of his vortices, it seems certain that downflow is common in the core of a waterspout (Golden 1973) and must be assumed likely to occur in a good many tornadoes (Morton 1966), although not necessarily immediately above the lower boundary.

If the dependence on surface drag as displayed by the model vortices is characteristic of these atmospheric vortices, as seems to us plausible, it is clear that the observed difference in strength between an average tornado and an average waterspout cannot be attributed to the different nature of the lower boundary and is probably a result of the presence of stronger forcing and possible a higher level of ambient rotation in most cases of tornado formation.

Acknowledgments

We are greatly indebted to Professor B. R. Morton of Monash University and Dr. J. S. Turner of Cambridge University for much stimulating discussion.

Two of us (L. B. and L. M. L.) express our gratitude to the Meteorological Office at Bracknell which provided the computing facilities. In particular Francis Hayes of Met. 0.11 gave us a great deal of expert programming assistance.

References

Bode, L. 1973 Ph.D. Thesis, University of Edinburgh.

Brooks, E. M. 1951 'Tornadoes and related phenomena,' *Compendium of Meteorology*, p. 673. Amer. Met. Soc.

Davies-Jones, R. P. and Vickers, G. T. 1971 'Numerical simulation of convective vortices,' NOAA Tech. Memo. ERL NSSL-57.

Dessens, J. 1972 'Influence of ground roughness on tornadoes: a laboratory simulation,' *J. Appl. Met.* **11**, pp. 72–75.

Fitzgarrald, D. E. 1973 'A laboratory simulation of convective vortices,' *J. Atmos. Sci.*, **30**, pp. 894–902.

Emmons, H. W. and Ying, S. J. 1967 'The fire whirl,' *Proc. Eleventh Symposium Combustion*. The Combustion Institute, pp. 475–488.

Golden, J. H. 1968 'Waterspouts at Lower Matecumbe Key, Florida, September 2, 1967,' *Weather*, **23**, pp. 103–114.

1971 'Waterspouts and tornadoes over south Florida,' *Mon. Weath. Rev.*, **99**, pp. 146–153.

1973 'The life and death of a waterspout,' *New Scientist*, **58**, pp. 665.

Leslie, L. M.	1971	'The development of concentrated vortices: a numerical study,' *J. Fluid Mech.*, **48**, pp. 1–21.
Long, R. R.	1958	'Vortex motion in a viscous fluid,' *J. Met.*, **15**, pp. 108–112.
Morton, B. R.	1966	'Geophysical vortices,' *Process in Aeronautical Sciences*, **7**, pp. 145–194 (ed. D. Küchemann). Pergamon.
	1969	'The strength of vortex and swirling core flows,' *J. Fluid Mech.*, **38**, pp. 315–333.
Rosenthal, S. L.	1971	'The response of a tropical cyclone model to variations in boundary layer parameters, initial conditions, lateral boundary conditions and domain size', *Mon. Weath. Rev.*, **99**, pp. 767–777.
Turner, J. S.	1966	'The constraints imposed on tornado-like vortices by the top and bottom boundary conditions, *J. Fluid Mech.*, **25**, pp. 377–400.
Turner, J. S. and Lilly, D. K.	1963	'The carbonated-water tornado vortex,' *J. Atmos. Sci.*, **20**, pp. 468–471.
Wan, C. A. and Chang, C. C.	1972	'Measurement of the velocity field in a simulated tornado-like vortex using a three-dimensional velocity probe,' *Ibid.*, **29**, pp. 116–127.
Ward, N. B.	1972	'The exploration of certain features of tornado dynamics using a laboratory model,' *Ibid.*, **29**, pp. 1194–1204.
Williams, G. P.	1967	'Thermal convection in a rotating fluid annulus, Part I,' *Ibid.*, **24**, pp. 144–161.
Ying, S. J. and Chang, C. C.	1970	'Exploratory model study of tornado-like vortex dynamics,' *Ibid.*, **27**, pp. 3–14.